Third-order theory of the Risley-prism-based beam steering system

Yajun Li

P.O. Box 975, Great River, New York 11739 (yajun_li@yahoo.com)

Received 6 October 2010; revised 17 November 2010; accepted 22 November 2010; posted 23 November 2010 (Doc. ID 136217); published 4 February 2011

Nonparaxial ray tracing is performed to investigate the field scanned out by a single beam through two rotatable thick prisms with different parameters, and a general solution is obtained and then expanded into a power series to establish the third-order theory for Risley prisms that paves the way to investigate topics of interest such as optical distortions in the scan pattern and an analytical solution of the inverse problem of a Risley-prism-based laser beam steering system; i.e., the problem is concerned with how to direct a laser beam to any specified direction within the angular range of the system.

OCIS codes: 080.0080, 080.2720, 120.5800, 220.2740.

1. Introduction

Risley prisms are pairs of rotatable wedge prisms that can be used to continuously scan a laser beam over a wide angular range with a high resolution [1]. Risley prisms are particularly useful in optical tracking and pointing a target in free space [2–4]. Figure 1 is a schematic diagram illustrating their configuration, in which the two prisms Π_1 and Π_2 may have different indices n_1 and n_2 and different apex angles α_1 and α_2.

By controlling the orientations, rate of rotation, and phasing of Π_1 and Π_2, many different scan patterns can be generated [4]. The thin prism approximation has been used for a first-order analysis, and it is found that the key parameter for the scan pattern generated by a pair of rotating prisms is the angular deviation between the incident and emerging rays of the prism [1,4]. For prisms Π_1 and Π_2, this key parameter can be expressed as

$$\delta_q = (n_q - 1)\alpha_q \qquad (q = 1, 2). \tag{1.1}$$

This study is organized as follows. Analytical ray tracing through the two-prism system is performed in Section 2 under the basis of the more exact thick prism theory; an exact solution of the scan field is obtained and then expanded into a power series of δ_q to give the closed-form approximations. Predictions of different order approximations are compared numerically, and the optical distortion in the scan pattern is investigated within the accuracy of third-order theory. A closed-form solution is developed in Section 3 for the inverse problem about how to direct a laser beam into any specified direction within the angular range of the Risley beam steering system [5]. Conclusions from this study are drawn at the end of this study.

This study starts with an error-free assumption: no prism tilt and no beam and mechanical axes misalignment will be considered throughout this study.

2. Exact and Approximate Expressions for the Scan Field

Figure 1 shows the three coordinate systems for ray tracing: (i) the coordinates (x, y, z) system with the triad $(\hat{\mathbf{i}}, \hat{\mathbf{j}}, \hat{\mathbf{k}})$ provides a Newtonian frame of reference, (ii) the coordinates (ξ, η) system is used for the convenience of incident beam profile definition, and (iii) the coordinates (X, Y) system for the plane of observation, on which the scan pattern is shown.

The two prisms Π_1 and Π_2, separated by an air gap d_{air}, are arranged with their flat sides together and in the positions perpendicular to the z axis, which is also the axis of rotation. The first surface of Π_1 (i.e.,

0003-6935/11/050679-08$15.00/0

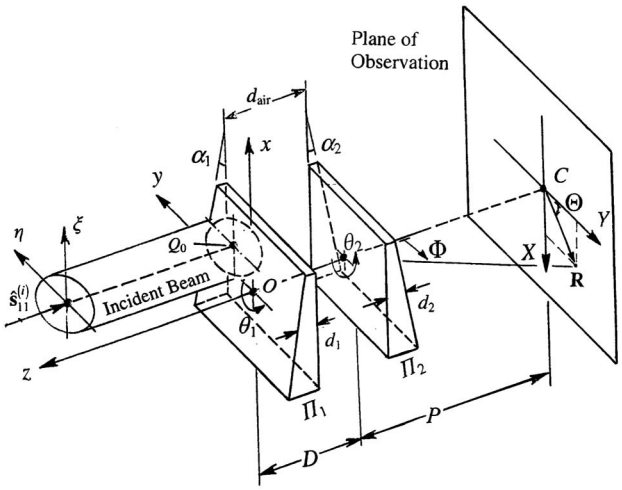

Fig. 1. Schematic diagram illustrating the notation and coordinate systems for ray tracing through Risley prisms. The incident beam is collinear with the z axis, which is also the axis of rotation of the two prisms Π_1 and Π_2 of indices n_1 and n_2 and apex angles α_1 and α_2, respectively.

the surface 11, for short) intersects the z axis at the origin point O of the (x,y,z) system. The thicknesses of Π_1 and Π_2 are, respectively, d_1 and d_2 as measured along the z axis. Rotations of the two prisms are described by

$$\theta_q = \omega_q t + \theta_{0q} \qquad (q = 1,2), \tag{2.2}$$

where t denotes time, ω_1 and ω_2 are angular frequencies of rotation, and θ_{01} and θ_{02} are the epoch phase angles. Assume $\theta_{01} = \theta_{02} = 0$ in all numerical calculations unless otherwise stated. To express the results more compactly, the following symbols will be used:

$$D = d_1 + d_{\text{air}} + d_2, \qquad D_n = \frac{d_1}{n_1} + d_{\text{air}} + \frac{d_2}{n_2}, \tag{2.3}$$

$$m = \omega_2/\omega_1. \tag{2.4}$$

The suffixes 11, 12, 21, and 22 will be attached to the symbols used in this study to show their relationships with the first or the second surface of prism Π_1 or Π_2.

Consider now that a single beam propagates to surface 11 in the direction specified by the unit vector $\hat{\mathbf{s}}_{11}^{(i)} = (0,0,-1)$. The beam is considered as a bundle of collimated rays perpendicular to the Oxy plane, and the beam axis passes through the point $Q_0(x_0,y_0)$ (see Fig. 1). In the case of scanning an elliptical beam with the major and minor axes ξ_0 and η_0, we can write the parametric expression for the incident beam as

$$\xi = x_0 + \xi_0 \cos\tau \quad \text{and} \quad \eta = y_0 + \eta_0 \sin\tau. \tag{2.5}$$

where τ is a parameter running from 0 to 2π.

The scan pattern is expressed in the coordinates (X,Y) system on the plane of observation located at a distance $(P+D)$ away from the origin O of the (x,y,z) system. It is known from a number of publications [1,6] that the pattern scanned out by a single ray through a pair of rotatable thin prisms on the (X,Y) plane located in the far-field region (i.e., where $P \gg D$) and perpendicular to the axis of the system can be expressed parametrically in the form

$$\begin{pmatrix} X \\ Y \end{pmatrix} = P\left[\delta_1 \begin{pmatrix} \cos\theta_1 \\ \sin\theta_1 \end{pmatrix} + \delta_2 \begin{pmatrix} \cos\theta_2 \\ \sin\theta_2 \end{pmatrix}\right]. \tag{2.6}$$

We may express Eq. (2.6) more compactly by using the complex vector

$$\mathbb{R}_{1F} = X + iY = P[\delta_1 \exp(i\theta_1) + \delta_2 \exp(i\theta_2)], \tag{2.7}$$

where $i = \sqrt{-1}$ and the suffix $1F$ to the symbol $\mathbb{R}$ stresses the fact that Eq. (2.7) is merely the first-order approximation to the scan pattern observed in the far-field region. Equation (2.7) will be referred to as the J&W formula because the book by Jenkins and White [6] provides easy access.

A. Analytical Ray Tracing and Exact and Approximate Expressions for the Scan Pattern

The parallelism between (ξ,η) and (x,y) (see Fig. 1) allows us to express the object points by the position vector

$$\mathbf{r}_{10} = (\xi,\eta,0). \tag{2.8}$$

The rectilinear propagation of the ray in the direction specified by $\hat{\mathbf{s}}_{11}^{(i)} = (0,0,-1)$ allows us to express the incident beam in the form

$$\hat{\mathbf{s}}_{11}^{(i)} \times (\mathbf{r} - \mathbf{r}_{10}) = 0, \tag{2.9}$$

where $\mathbf{r} = (x,y,z)$ is the position vector for a typical point on the cross section of the incident beam. The next step is to determine $\mathbf{r}_{11} = (x_{11},y_{11},z_{11})$, which is the position vector for the points where the beam strikes surface 11 in the position specified by the unit normal

$$\hat{\mathbf{n}}_{11} = (\sin\alpha_1 \cos\theta_1, \sin\alpha_1 \sin\theta_1, \cos\alpha_1), \tag{2.10}$$

Because the origin O of the coordinates (x,y,z) system is on surface 11, we may therefore express surface 11 as

$$\hat{\mathbf{n}}_{11} \cdot \mathbf{r} = 0. \tag{2.11}$$

Solve Eqs. (2.9) and (2.11) simultaneously for the position vector $\mathbf{r}_{11}$ to ascertain where the incident beam strikes surface 11 and then is refracted into the beam propagating in the direction specified by the ray vector $\hat{\mathbf{s}}_{11}^{(r)} = (K_{11}^{(r)}, L_{11}^{(r)}, M_{11}^{(r)})$. The two ray vectors $\hat{\mathbf{s}}_{11}^{(i)}$ and $\hat{\mathbf{s}}_{11}^{(r)}$ are coupled by the Snell law [7]. From air to glass, we can write the Snell law as

$$\hat{\mathbf{s}}_{11}^{(r)} = \frac{1}{n_1}[\hat{\mathbf{s}}_{11}^{(i)} - (\hat{\mathbf{s}}_{11}^{(i)} \cdot \hat{\mathbf{n}}_{11})\hat{\mathbf{n}}_{11}] - (\hat{\mathbf{n}}_{11})\sqrt{1 - \left(\frac{1}{n_1}\right)^2 + \left(\frac{1}{n_1}\right)^2 (\hat{\mathbf{s}}_{11}^{(i)} \cdot \hat{\mathbf{n}}_{11})^2}. \quad (2.12)$$

Equations (2.8), (2.9), (2.10), and (2.11) can be extended to describe the ray transfer from surface 11 to surface 12 by changing the suffixes $11 \rightarrow 10$ and $12 \rightarrow 11$ to the symbols used in these equations. It would be ready for the next calculation of refraction at the boundary surface 12. The unit vectors $\hat{\mathbf{s}}_{12}^{(i)}$ and $\hat{\mathbf{s}}_{12}^{(r)}$ for the rays before and after refraction at the boundary surface 12 from glass to air are coupled by the Snell law in the form

$$\hat{\mathbf{s}}_{12}^{(r)} = n_1[\hat{\mathbf{s}}_{11}^{(r)} - (\hat{\mathbf{s}}_{11}^{(r)} \cdot \hat{\mathbf{n}}_{12})\hat{\mathbf{n}}_{12}] - (\hat{\mathbf{n}}_{12})\sqrt{1 - n_1^2 + n_1^2(\hat{\mathbf{s}}_{11}^{(r)} \cdot \hat{\mathbf{n}}_{12})^2}. \quad (2.13)$$

Applying the formulation and sign convention continuously to cross the air gap, then to the first surface of the second prism Π_2 (i.e., surface 21) and to surface 22, we will obtain the position vector $\mathbf{r}_{22} = (x_{22}, y_{22}, z_{22})$ and the ray vector $\hat{\mathbf{s}}_{22}^{(r)} = (K_{22}^{(r)}, L_{22}^{(r)}, M_{22}^{(r)})$, which are the two parameters to determine the beam emerging from the system. After a long derivation, omitted here, we found the direction cosines of the emerging beam, given by

$$\left.\begin{aligned} K_{22}^{(r)} &= \sin\alpha_1\left(\cos\alpha_1 - \sqrt{n_1^2 - \sin^2\alpha_1}\right)\cos\theta_1 + A\sin\alpha_2\cos\theta_2, \\ L_{22}^{(r)} &= \sin\alpha_1\left(\cos\alpha_1 - \sqrt{n_1^2 - \sin^2\alpha_1}\right)\sin\theta_1 + A\sin\alpha_2\sin\theta_2, \\ M_{22}^{(r)} &= -\sqrt{n_2^2 - n_1^2 + \left[\sin^2\alpha_1 + \cos\alpha_1\sqrt{n_1^2 - \sin^2\alpha_1}\right]^2} - A\cos\alpha_2 \end{aligned}\right\}, \quad (2.14)$$

where

$$A = \sqrt{1 - n_2^2 + \left[\begin{aligned} &\cos\alpha_2\sqrt{n_2^2 - n_1^2 + \left[\sin^2\alpha_1 + \cos\alpha_1\sqrt{n_1^2 - \sin^2\alpha_1}\right]^2} \\ &+ \sin\alpha_1\sin\alpha_2\left(\cos\alpha_1 - \sqrt{n_1^2 - \sin^2\alpha_1}\right)\cos(\theta_2 - \theta_1)\end{aligned}\right]^2}$$

$$- \cos\alpha_2\sqrt{n_2^2 - n_1^2 + \left[\sin^2\alpha_1 + \cos\alpha_1\sqrt{n_1^2 - \sin^2\alpha_1}\right]^2} - \sin\alpha_1\sin\alpha_2\left(\cos\alpha_1 - \sqrt{n_1^2 - \sin^2\alpha_1}\right)\cos(\theta_2 - \theta_1).$$

The scan vector $\mathbf{R}$ with one end at the point specified by the position vector $\mathbf{r}_{22}$ and the other end at the observation plane located at $z = P + D$ describes the scan pattern {see, e.g., Eq. (18) in [8]}:

$$\mathbf{R} = \mathbf{r}_{22} - \frac{(P + D) + \hat{\mathbf{k}} \cdot \mathbf{r}_{22}}{\hat{\mathbf{k}} \cdot \hat{\mathbf{s}}_{22}^{(r)}}\hat{\mathbf{s}}_{22}^{(r)}. \quad (2.15)$$

where $\mathbf{r}_{22}$ is a function of the parameters D, D_n, and $(x_0, y_0; \xi_0, \eta_0)$. The expression for $\mathbf{r}_{22}$ is too long to show here, but it can be obtained from the author on request. However, $\mathbf{r}_{22}$ becomes negligible in the far-field region where $P \gg |\mathbf{r}_{22}|$ and $\gg D$. On these conditions, all the terms containing D, D_n, and $(x_0, y_0; \xi_0, \eta_0)$ in Eq. (2.15) can be discarded, and then the two components (X, Y) of the scan vector $\mathbf{R}$ in Eq. (2.15) are given by

$$\begin{pmatrix} X \\ Y \end{pmatrix} = -P\frac{\sin\alpha_1\left(\cos\alpha_1 - \sqrt{n_1^2 - \sin^2\alpha_1}\right)\begin{pmatrix}\cos\theta_1 \\ \sin\theta_1\end{pmatrix} + A\sin\alpha_2\begin{pmatrix}\cos\theta_2 \\ \sin\theta_2\end{pmatrix}}{\sqrt{n_2^2 - n_1^2 + \left[\sin^2\alpha_1 + \cos\alpha_1\sqrt{n_1^2 - \sin^2\alpha_1}\right]^2} + K_{22}\cos\alpha_2}, \quad (2.16)$$

or expressed more compactly as

$$\mathbb{R} = X + iY = -P\frac{\sin\alpha_1(\cos\alpha_1 - \sqrt{n_1^2 - \sin^2\alpha_1})\exp(i\theta_1) + A\sin\alpha_2\exp(i\theta_2)}{\sqrt{n_2^2 - n_1^2 + \left[\sin^2\alpha_1 + \cos\alpha_1\sqrt{n_1^2 - \sin^2\alpha_1}\right]^2} + K_{22}\cos\alpha_2}. \quad (2.17)$$

Attention is now turned to a discussion of the different order closed-form approximations to the exact solution.

B. Third-Order Approximation

When all the terms of an order higher than α^3 in the power expansion of Eq. (2.15) are discarded, we obtain the third-order approximation to the exact solution in the form

$$\begin{aligned}\mathbb{R}_3 = \mathbb{R}_{1F} + P\Bigg\{ &\left[\frac{3n_1^3 - 6n_1^2 + 2n_1 + 3}{6n_1(n_1-1)^2}\delta_1^3\right. \\ &+ \frac{2n_2 - 1 + n_2\exp[2i(\theta_2-\theta_1)]}{2(n_2-1)}\delta_1\delta_2^2\Bigg]\exp(i\theta_1) \\ &+ \left[\frac{2n_2 + 1 + n_2\exp[2i(\theta_1-\theta_2)]}{2n_2}\delta_1^2\delta_2\right. \\ &\left.\left.+ \frac{3n_2^2 - 3n_2 + 2}{6(n_2-1)^2}\delta_2^3\right]\exp(i\theta_2)\right\} + \mathbb{R}_{3N}, \end{aligned} \tag{2.18}$$

where $\mathbb{R}_{1F}$ represents the so-called J&W formula as shown in Eq. (2.7) and

$$\begin{aligned}\mathbb{R}_{3N} = &-\rho_{10} - \frac{\delta_1^2}{n_1(n_1-1)}g(\theta_1)\exp(i\theta_1) \\ &+ g(\theta_2)\left[\frac{\delta_1}{n_2}\exp(i\theta_1) + \frac{\delta_2}{n_2-1}\exp(i\theta_2)\right]\delta_2 \\ &+ D_n\Bigg[\Bigg(1 + \frac{2n_1^2 - 3n_1 + 3}{6n_1^2(n_1-1)^2}\delta_1^2 \\ &+ \frac{n_2+1}{n_2(n_2-1)}\delta_1\delta_2\cos(\theta_1-\theta_2)\Bigg)\delta_1\exp(i\theta_1) \\ &+ \frac{\delta_1\delta_2^2\cos(\theta_1-\theta_2)}{n_2-1}\exp(i\theta_2)\Bigg], \end{aligned} \tag{2.19}$$

where $\rho_{10} = \xi + i\eta$ and $g(\theta) = x_{10}\cos\theta + y_{10}\sin\theta$. Equation (2.18) is valid in both the near- and far-field regions, in which the term $\mathbb{R}_{3N}$ represents contributions of D_n and $(x_0, y_0; \xi_0, \eta_0)$ to the scan pattern as observed in the near-field region and can be neglected in the far-field region.

C. Second-Order Theory

When all the terms of an order higher than δ^2 in Eq. (2.19) are discarded, we obtain the second-order approximation to the exact solution that is valid in both the near- and far-field regions and can be expressed in the form

$$\begin{aligned}\mathbb{R}_2 = \mathbb{R}_{1F} - \rho_{10} + \delta_1\left[D_n - \frac{\delta_1}{n_1(n_1-1)}g(\theta_1)\right]\exp(i\theta_1) \\ + \delta_2\left[\frac{\delta_1}{n_2}\exp(i\theta_1) + \frac{\delta_2}{n_2-1}\exp(i\theta_2)\right]g(\theta_2). \end{aligned} \tag{2.20}$$

D. First-Order Approximation

When all the terms of an order higher than δ^1 in Eq. (2.20) are discarded, there remains the first-order approximation to the exact solution that is valid in both the near- and far-field regions and can be expressed in the form

$$\begin{aligned}\mathbb{R}_1 = P[\delta_1\exp(i\theta_1) + \delta_2\exp(i\theta_2)] - \rho_{10} \\ + D_n\delta_1\exp(i\theta_1). \end{aligned} \tag{2.21}$$

When the pattern is scanned out by a single ray collinear with the z axis, i.e. when $\rho_{10} = 0$, Eq. (2.21) reduces to the form

$$\mathbb{R}_1 = P\left[\delta_1\left(1 + \frac{D_n}{P}\right)\exp(i\theta_1) + \delta_2\exp(i\theta_2)\right]. \tag{2.22}$$

In the far-field region, Eqs. (2.21) and (2.22) reduce to the J&W formula shown in Eqs. (2.7).

E. Numerical Comparison of the Exact Solution and the Predictions of Approximate Theories

The curves in Figs. 2(a)–2(d) are plotted from Eqs. (2.16), (2.17), (2.18), (2.19), (2.20), and (2.22) for a comparison of the predictions of the exact solution and approximate theories for the patterns scanned out by a single ray through Risley prisms having two identical prisms of apex angle $\alpha = 0°\ldots30°$ and index $n = 1.5$. Scan patterns are displayed either on the plane in the far-field region ($D/P \to 0$) or on planes in the near-field region at different distances $D/P = 0.15$, 0.3, and 0.45. In Figs. 2(a)–2(d), a comparison was performed under the condition of $\theta_1 = \theta_2 = 0$. This is because a pair of rotatable prisms is equivalent to a single prism of variable power that reaches the maximum when the two prisms are in parallel.

The two curves in Fig. 2(a) show the percentage difference $\Delta(\%)$ between the predictions of approximate theories of different order compared with the predictions of the exact solution. In the far-field region, the J&W formula, the first- and second-order approximations give the same numerical results and can therefore be shown by one curve to compare with the curve plotted from Eq. (2.18) for the third-order theory. Numerical results are also shown in Table 1, and we see that the scan pattern predicted by the first- and second-order theories may have ~1% maximum error when the apex angle $\alpha = 5°$ as compared with the prediction of the exact solution, whereas, under the same condition, the error reduces drastically to ~0.01% for the prediction by the third-order theory. The curves in Figs. 2(b)–2(d) show a comparison of scan patterns displayed on planes in the near-field range. Similar conclusions can be drawn that the third-order approximation has much higher accuracy than the predictions by the first-order theory.

It is known from a number of publications [1,4] that a line scan can be produced by two counter-rotated prisms at equal velocities, i.e., when the ratio

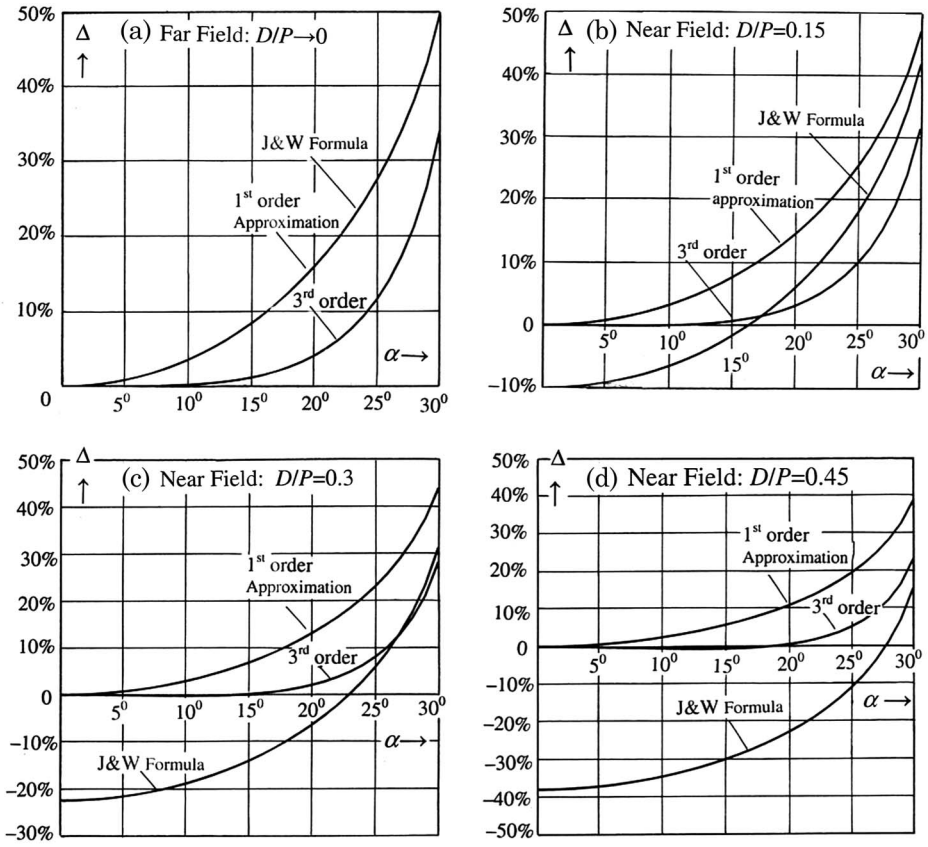

Fig. 2. Curves plotted from Eqs. (2.16), (2.17), (2.18), (2.19), (2.20), and (2.22) under the condition of $\theta_1 = \theta_2 = 0$ for a comparison of the percentage difference $\Delta(\%)$ in the calculations of the patterns scanned out by a single ray through Risley prisms having two identical prisms of index $n = 1.5$ and the apex angle of $\alpha = 0°\ldots30°$ on a plane in the far-field region ($D/P \to 0$) and planes at different distances $D/P = 0.15$, 0.3, and 0.45 in the near-field region.

of angular frequencies $m = -1$. Figure 3(b) show that the line scan on plane in the far-field region is the prediction of the first-order theory, whereas the exact solution and the third-order theory predict a bow-tie scan. In the near-field region, all the theories predict a long elliptical pattern, as shown in Fig. 3(a).

Figures 4(a) and 4(b) show the predictions of the third-order theory [see Eq. (2.18)] about the distortions of the scanning spot in the far-field region when the incident beams with either a circular or an elliptical profile. It is seen from Figs. 4(a) and 4(b) that there is no distinct deformation or spot rotation when the spot is tracing along the three-petal-rose curve produced by a pair of counter-rotated prisms when the ratio of angular frequencies $m = -2$.

3. Third-Order Solution of the Inverse Problem

Directing a laser beam to any specified altitude angle Φ and azimuth angle Θ within the angular range of the Risley prisms is known as the inverse problem of the Risley-prism-based laser beam steering system (see, e.g., [5] and references cited therein). Compared to the existing results, a concise and closed-form solution to the inverse problem will be presented in this section within the accuracy of the third-order theory.

First, we return to Eq. (2.14) and show the third-order expressions of the direction cosines for the beam emergent from the system as

$$K_{22}^{(r)} = -(\delta_1 \cos\theta_1)\kappa_1 - (\delta_2 \cos\theta_2)\kappa_2, \tag{3.1a}$$

$$L_{22}^{(r)} = -(\delta_1 \sin\theta_1)\kappa_1 - (\delta_2 \sin\theta_2)\kappa_2, \tag{3.1b}$$

$$M_{22}^{(r)} \approx -1 + \frac{\delta_1^2}{2} + \frac{\delta_2^2}{2} + \delta_1\delta_2 \cos(\theta_2 - \theta_1), \tag{3.1c}$$

where

$$\kappa_1 = 1 + \frac{3 - n_1}{6n_1(n_1 - 1)^2}\delta_1^2, \tag{3.2a}$$

$$\kappa_2 = 1 + \frac{\delta_1^2}{2n_2} + \frac{3n_2 - 1}{6(n_2 - 1)^2}\delta_2^2 + \frac{\delta_1\delta_2 \cos(\theta_2 - \theta_1)}{n_2 - 1}. \tag{3.2b}$$

Table 1. Percentage Error of the Approximate Formulas Eqs. (2.18), (2.20), and (2.22) of Different Orders as Compared with the Prediction of the Exact Solution in Eq. (2.16) under the Condition of $\theta_1 = \theta_2 = 0$

$\alpha =$	0°	5°	10°	15°	20°	25°	30°
J&W formula, first- and second-order approximation	0	0.9%	3.7%	8.5%	16.1%	27.9%	51.3%
Third-order approximation	0	0.01%	0.23%	1.2%	4.2%	11.9%	35.8%

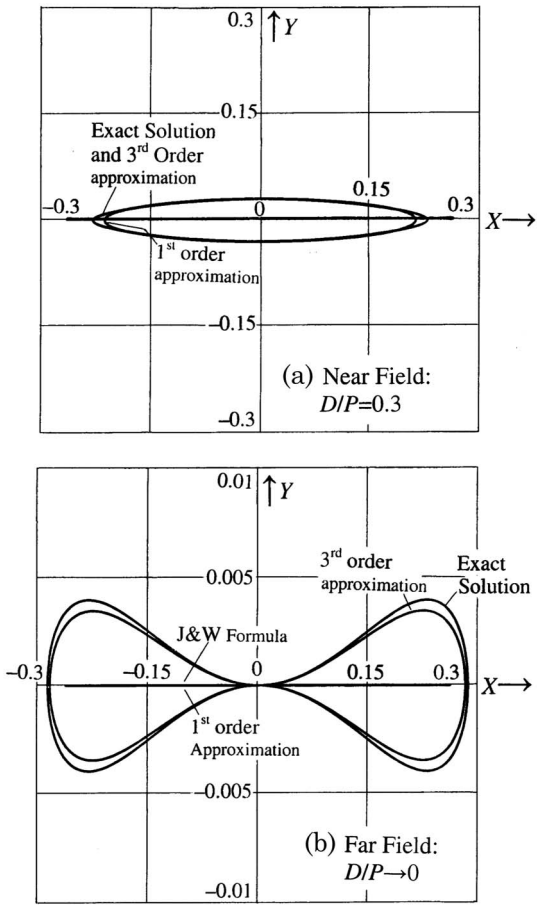

Fig. 3. Distortions of line scan patterns produced by two prisms counter-rotated at equal angular velocities. The prisms are identical with index $n = 1.5$ and apex angle $\alpha = 15°$: (a) near-field and (b) far-field region scan patterns.

To steer the beam into the desired direction, the first step is to rotate the second prism Π_2 relative to the first prism Π_1 until the desired altitude is achieved, i.e.,

$$\cos\Phi = -M_{22}^{(r)} = 1 - \frac{\delta_1^2}{2} - \frac{\delta_2^2}{2} - \delta_1\delta_2\cos(\Delta\theta)_0, \quad (3.3)$$

where $(\Delta\theta)_0 = \theta_2 - \theta_1$ represents the angle of relative rotation. After some rearranging,

$$(\Delta\theta)_0 = \arccos\left[\frac{2(1-\cos\Phi) - (\delta_1^2 + \delta_2^2)}{2\delta_1\delta_2}\right]. \quad (3.4)$$

The curves in Fig. 5(a) are plotted from Eq. (3.4) to show the one-to-one correspondence between Φ and $(\Delta\theta)_0$ in systems containing two identical prisms of index $n = 1.5$ and a different prism angle α ranging from 2.5° to 10°.

After the desired altitude is achieved, the azimuth of the beam emerging from the system is given by

$$\psi_0 = \arctan\left(\frac{L_{22}^{(r)}}{K_{22}^{(r)}}\right)_{\substack{\theta_1 = 0,\\ \theta_2 = (\Delta\theta)_0}}. \quad (3.5)$$

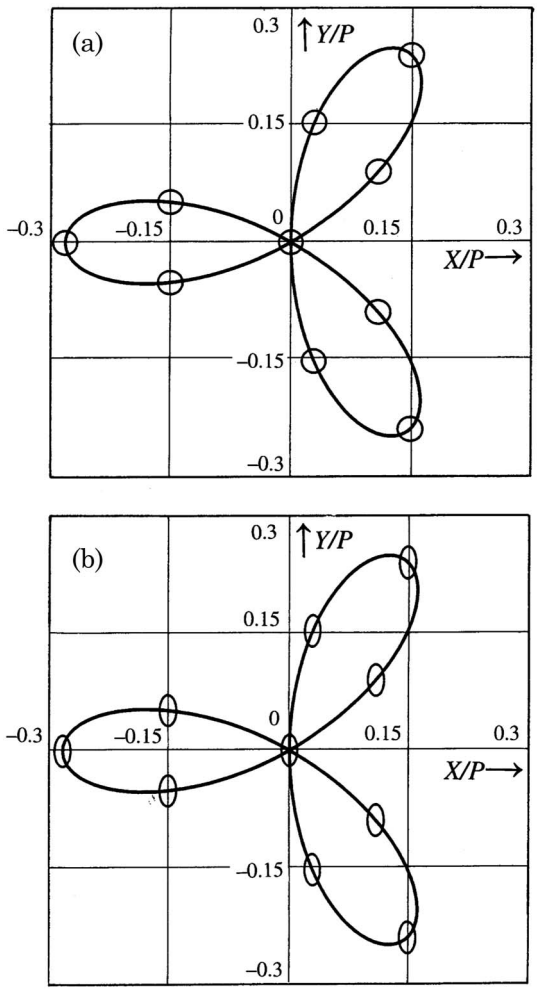

Fig. 4. Far-field region scan patterns predicted by the third-order theory to show the scanning spot along the three-petal-rose curve produced by a pair of identical prisms of $n = 1.5$, apex angle $\alpha = 15°$ and counter-rotated with the angular frequency ratio $m = -2$. Incident beam with (a) circular profile of radius 0.015 P and (b) elliptical profile with the major and minor axes (0.02 P, 0.01 P).

Upon substituting from Eqs. (3.1a), (3.1b), and (3.2) into Eq. (3.5), we arrive at

$$\left(\frac{L_{22}^{(r)}}{K_{22}^{(r)}}\right)_{\substack{\theta_1=0,\\ \theta_2=(\Delta\theta)_0}} = \frac{\kappa_{20}\sqrt{4\delta_1^2\delta_2^2 - [2(1-\cos\Phi) - (\delta_1^2+\delta_2^2)]^2}}{2\kappa_1\delta_1^2 + \kappa_{20}[2(1-\cos\Phi) - (\delta_1^2+\delta_2^2)]}, \quad (3.6)$$

where

$$\kappa_{20} = \kappa_2\Big|_{\substack{\theta_1=0,\\ \theta_2=(\Delta\theta)_0}} = 1 + \frac{\delta_1^2}{2n_2} + \frac{3n_2-1}{6(n_2-1)^2}\delta_2^2 + \frac{2(1-\cos\Phi) - (\delta_1^2+\delta_2^2)}{2(n_2-1)}. \quad (3.7)$$

Again, upon substituting from Eq. (3.7) into Eq. (3.6) and then into Eq. (3.5) and then discarding all the terms of an order higher than δ^3, there remains

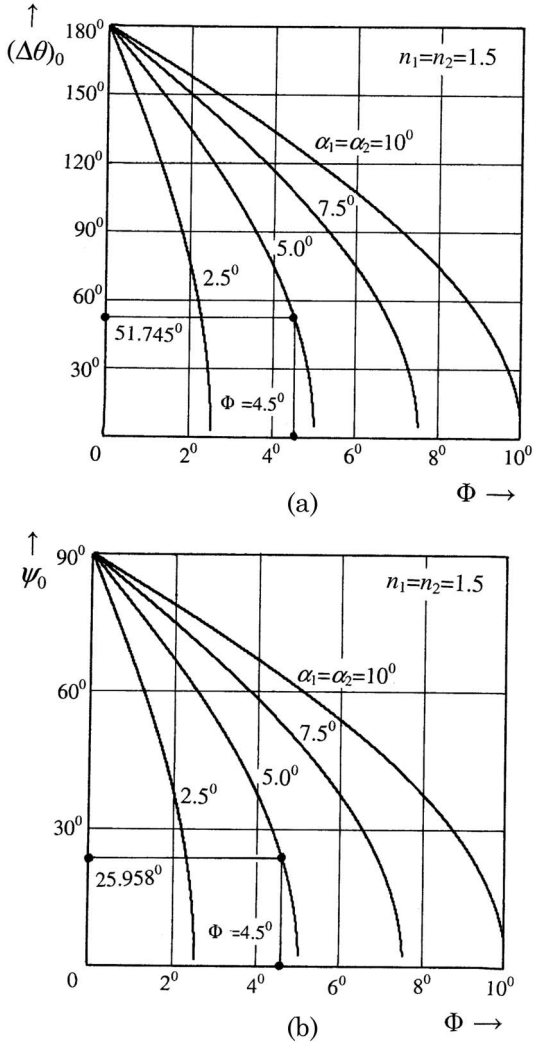

Fig. 5. Curves plotted under the condition of two identical prisms of index $n = 1.5$ and different apex angle α ranging from 2.5° to 10° to show the third-order solution of the inverse problem, i.e., to direct a laser beam to the desired altitude Φ and azimuth Θ. (a) Curves, plotted from Eq. (3.4), showing the dependence of the azimuth rotation angle $(\Delta\theta)_0$ between the two prisms on the desired altitude Φ, (b) Curves, plotted from Eq. (3.8), showing the azimuth ψ_0 of the beam after the desired altitude is achieved.

$$\psi_0 = \arctan \times \left\{ \frac{(n_2 - \cos\Phi)\sqrt{4\delta_1^2\delta_2^2 - [2(1-\cos\Phi) - (\delta_1^2+\delta_2^2)]^2}}{(n_2-1)\delta_1^2 + (n_2-\cos\Phi)[2(1-\cos\Phi) - (\delta_1^2+\delta_2^2)]} \right\}. \tag{3.8}$$

The curves in Fig. 5(b) are plotted from Eq. (3.8) under the same conditions for Fig. 5(a).

The second step is to rotate the two prisms together around the optical axis to reach the desired azimuth Θ. In the course of rotation, the beam emerging from the system will trace out the surface of a cone with a half-vertex angle Φ in space. The target, specified by altitude Φ and azimuth Θ, must be on the surface of the cone and can be reached by rotating the two prisms together to the angle $\Theta - \psi_0$. This means the final rotational angles of the two prisms are, respectively, given by

$$\theta_1 = \Theta - \psi_0 \quad \text{and} \quad \theta_2 = \theta_1 + (\Delta\theta)_0. \tag{3.9}$$

To this stage, a case example may be helpful to show the accuracy of the inverse solution provided by third-order theory. Assume a laser beam is required to steer to a target specified by altitude $\Phi = 4.5°$ and azimuth $\Theta = 120°$ by the Risley prisms having two identical prisms of index $n = 1.5$ and prism angle $\alpha = 5°$. We obtain from Eqs. (3.6) and (3.8) that $(\Delta\theta)_0 = 51.745°$ and $\psi_0 = 25.958°$ and then from Eq. (3.9) that

$$\theta_1 = 120° - 25.958° = 94.042°,$$

$$\theta_2 = 120° - 25.958° + 51.745° = 145.787°.$$

Accuracy can be estimated by inserting the numbers $\theta_1 = 94.042°$ and $\theta_2 = 145.787°$ back into Eq. (2.14) for the exact solutions of the direction cosines, and then we find $\Phi = 4.523°$ and the azimuth $\psi_0 = 25.961°$, which are very close to the values of $\Phi = 4.5°$ and $\psi_0 = 25.958°$ as predicted by Eq. (3.5).

4. Conclusions

In conclusion, nonparaxial ray tracing has been performed to investigate the structure of the scan field produced by a Risley-prism system with two thick prisms of different parameters. A power expansion of the exact result led to the establishment of the approximation theory of Risley prisms. The accuracy of the approximate theory of different orders has been compared numerically with the prediction of the exact solution. It is shown that the third-order approximation can be used to predict the optical distortions in the scan patterns and permits a simply and accurate solution to the inverse problem encountered in the application of Risley prisms to free-space communications.

The author thanks an anonymous referee who took time to call his attention to two important publications in the theory of rotating prisms published by Erfle [9] and Pogarev [10].

References

1. F. A. Rosell, "Prism scanners," J. Opt. Soc. Am. **50**, 521–526 (1960).
2. C. T. Amirault and C. A. DiMarzio, "Precision pointing using a dual-wedge scanner," Appl. Opt. **24**, 1302–1308 (1985).
3. M. Ostaszewski, S. Harford, N. Doughty, C. Hoffman, M. Sanchez, D. Gutow, and R. Pierce, "Risley prism beam pointer," Proc. SPIE **6304**, 630406 (2006).
4. W. L. Wolfe, "Optical-mechanical scanning techniques and devices," in *The Infrared Handbook*, W. L. Wolfe and G. J. Zissis, eds. (Environmental Research Institute of Michigan, 1989), Chap. 10.

5. Y. Yang, "Analytic solution of free space optical beam steering using Risley prisms," J. Lightwave Technol. **26**, 3576–3583 (2008).
6. F. R. Jenkins and H. E. White, *Fundamentals of Optics*, 4th ed. (McGraw-Hill, 2001), Sec. 2.7.
7. M. Born and E. Wolf, *Principles of Optics*, 7th ed. (Cambridge University, 1999), Sec. 3.2.2.
8. Y. Li and J. Katz, "Laser beam scanning by rotary mirrors. I. modeling mirror scanning devices," Appl. Opt. **34**, 6403–6416 (1995).
9. H. Erfle, "Über die durch ein Drehkeilpaar erzeugte Ablenkung und über eine als Kennzeichen für die Beibehaltung des 'Hauptschnittes' dienende Sinusbedingung," Zeitschrift für Physik **1**, 57–81 (1920).
10. http://vova1001.narod.ru/00009295.htm.